Measurement of H^-, H^0, and H^+ yields produced by foil stripping of 800-MeV H^- ions

M. S. Gulley, P. B. Keating, H. C. Bryant, E. P. MacKerrow, W. A. Miller, and D. C. Rislove
Department of Physics and Astronomy, University of New Mexico, Albuquerque, New Mexico 87131-1156

Stanley Cohen, J. B. Donahue, D. H. Fitzgerald, S. C. Frankle, David J. Funk, R. L. Hutson, R. J. Macek, M. A. Plum, N. G. Stanciu, O. B. van Dyck, and C. A. Wilkinson
Los Alamos National Laboratory, Los Alamos, New Mexico 87545

C. W. Planner
Rutherford Appleton Laboratory, Chilton, Didcot, Oxon OX1 10QX, United Kingdom
(Received 12 June 1995)

Measurements of H^- stripping and H^0 excited-state production for a wide range of foil thicknesses and experimental conditions are reported. An 800-MeV H^- beam was passed through carbon or aluminum oxide foils of thicknesses ranging from 10 to 550 $\mu g/cm^2$ and the excited states produced were analyzed by field stripping in a special magnet downstream of the foil. The foil thicknesses were independently determined. The H^0 atoms emerging in excited states with $n>2$ can be stripped to protons in fields of up to 1.3 T. The yield of excited states as a function of foil thickness and the cross sections for the various interactions are presented. The cross-section ratio of double to single ionization of H^- in carbon is found to be $(1.8\pm0.9)\%$.

PACS number(s): 34.50.Fa

I. INTRODUCTION

Intense perturbations with very rapid onset and turn off, persisting for up to several femtoseconds, are applied to relativistic H^- ions passing through a thin foil. Can the jumble of electromagnetic impulses received by this simple two-electron system be interpreted as a series of incoherent interactions with individual atoms? Are coherent interactions with several atoms, or indeed, an entire string of atoms involved? In order to study experimentally the nature of the interaction, we have continued a series of measurements [1] of the reaction products emerging from carbon foils through which 800-MeV H^- ions pass. A theoretical simulation of the transmission process can be found in the accompanying paper [2]. We have also made some initial studies with aluminum oxide (Al_2O_3) foils. We have determined the absolute ratio of production of protons and H^0 atoms, including excited states, and the attenuation of H^- as a function of the foil thickness. In this paper we report on the yields for the principal quantum states (shells) of hydrogen, designated by the quantum number n. From fits to rate equations we have interpreted our results in terms of atom-atom cross sections.

The present study was prompted by the problem of first-turn losses at the Proton Storage Ring at the Los Alamos Meson Physics Facility (LAMPF). All evidence to date supports the hypothesis that most of the observed first-turn losses are caused by the ring bending magnets field-ionizing excited-state H^0 atoms that are not stripped by the foil. These protons soon collide with the wall of the ring because they are produced at a point where their trajectories are outside the acceptance of the ring [3,4].

Our work differs from previous measurements of H^- beam-foil interactions at LAMPF [1] by the introduction of a linearly ramped magnetic field downstream of the beam-foil interaction region. This ramped field allows us to sort out the excited states of hydrogen, since each excited state is stripped of its electron at a different point in the motional field. The relative abundance of each state can be determined by the resulting distribution of proton trajectories. That the loosely bound H^- ion (with a binding energy of 0.754 eV), whose outer electron occupies a volume on the order of eight times that of the carbon atom, makes it through the foil intact at all is quite interesting (Fig. 1). Interaction times are on the order of 0.1–5.7 fs. When a beam of H^- ions passes through a foil, some ions are stripped of both electrons to become protons (H^+) with a stripping cross section of σ_{-+} some are stripped of one electron to become hydrogen atoms [$H^0(n)$] with a stripping cross section of σ_{-n}, and some pass through the foil unscathed. As Fig. 2 shows, there are other possible interactions, such as a H^0 in $n=1$ or 2 (in our measurements, we are unable to distinguish these) being excited to a higher state with an effective cross section σ_{12n}.

When the H^0 atoms enter a magnetic field, in their rest frame they are subjected to, in addition to the magnetic field, a motional electric field $F_{\rm ion}$ given by [5]

$$F_{\rm ion}=\gamma\beta c B_{\rm lab}, \tag{1}$$

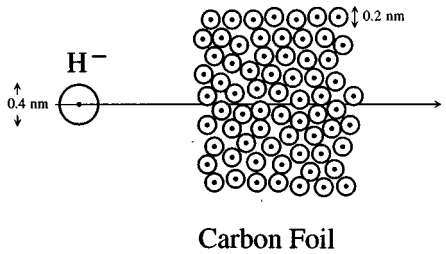

FIG. 1. The relative sizes of the outer electron orbits for the H^- ion and the carbon atoms comprising the foil. How can the H^- emerge intact?

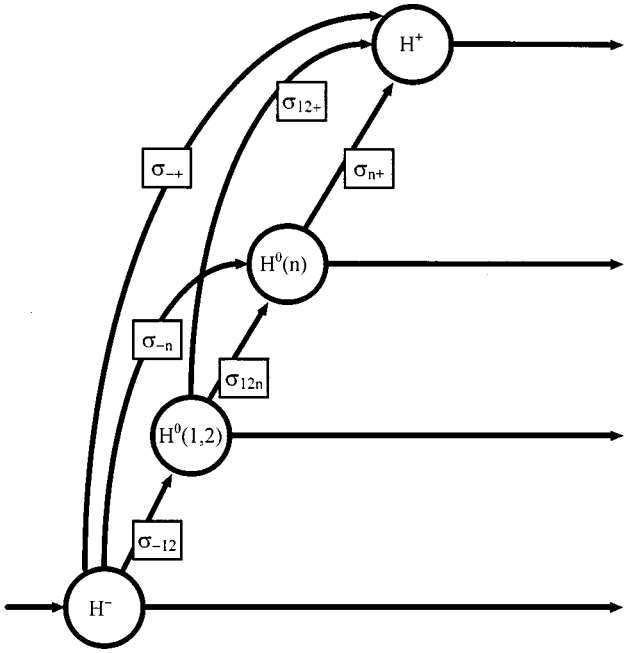

FIG. 2. Road map of the important interactions occurring when a relativistic H^- passes through matter. Collisions that lower the principal quantum number have not been considered.

where F is in V/m and B is in teslas. The ion velocity is perpendicular to $B_{\rm lab}$. The symbols γ and β are the usual relativistic parameters of the beam. For an 800-MeV H^- beam, $\beta=0.84$ and $\gamma=1.85$. Thus a magnetic field of 1 to transforms to an electric field of 4.7 MV/cm in the rest frame of the ion. This intense electric field causes the atom to become unstable since the electron can tunnel through the potential barrier. Ionization will proceed rapidly at a critical field (V/cm) given, to first order, by [6]

$$F_c = \frac{5.142\times 10^9}{9n^4}, \tag{2}$$

where n is the principal quantum number of the spherical states. The magnetic field used in this experiment is able to strip H^0 states with $n>2$. The linearly increasing field along the particles' path through the magnet allows us to trace the trajectories back to the field strength at which they stripped. This critical field strength then indicates the quantum state of the H^0 (Fig. 3).

We fit our measured yield curve in terms of simple rate calculations based on the assumption of one or more incoherent atom-atom interactions in the foil.

II. MODEL

It is instructive to consider a simple rate model of the interactions. A more detailed analysis of these phenomena using transport theory has been developed by Gervais, Reinhold, and Burgdörfer [2]. We assume that the H^- and its various stripped states interact with individual carbon atoms. The interactions are described in terms of cross sections. This model implicitly assumes that phases are not relevant from one interaction to the next as the ion and its products pass through the foil. In this sense, this model is incoherent, even though, as demonstrated in the accompanying theoretical analysis [2], collective effects must play a role. Our model is essentially that discussed by Mohagheghi *et al.* [1] with the addition of the possibility of a two-step process for $n\geqslant 3$. Our measurements do not distinguish between $n=1$ and 2 as the fields available were not strong enough to strip $n=2$.

Thus the probability $y_-(x)$ that the H^- remain intact after passage through an areal density x of foil material is given by

$$y_-(x) = Ae^{-\rho\sigma_- x}, \tag{3}$$

where A is nominally unity, although we retain it as a fitting parameter. σ_- is the sum of σ_{-0} and σ_{-+}, where σ_{-0} and σ_{-+} are the cross sections in cm^2 for one- and two-electron stripping, respectively, and ρ is the number of atoms per microgram of foil material.

Following Mohagheghi *et al.* [1], the probability of the appearance of a hydrogen in the $n=1$ or 2 state at x is

$$y_{1,2}(x) = AC(e^{-\sigma_{12}\rho x} - e^{-\sigma_-\rho x}), \tag{4}$$

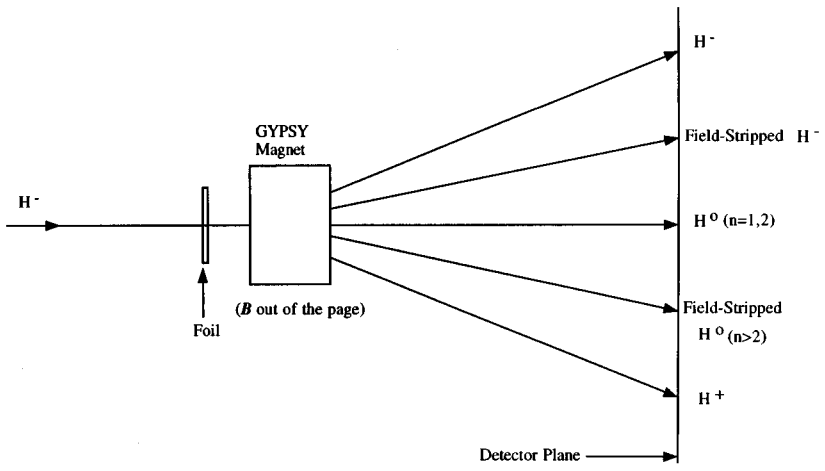

FIG. 3. The 800-MeV H^- beam is directed through a self-supported 2-cm-diam foil. The emerging excited states of hydrogen are sorted by the gradient-field magnet (labeled "gypsy" magnet); their trajectories reflect the strength of the required stripping field. H^0 ($n=1$ and 2) cannot be stripped by the field. Unstripped H^- and fully stripped H^+ are deflected maximally.

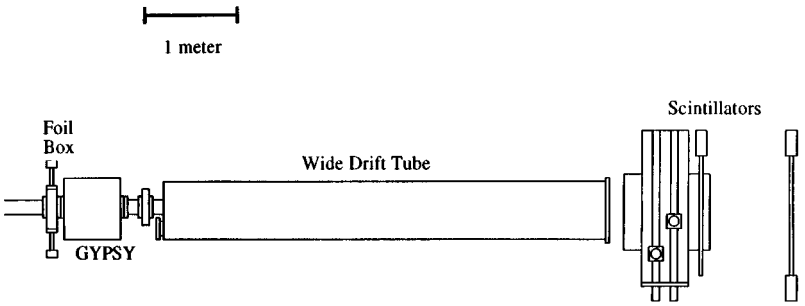

FIG. 4. The H^- beam enters from the left. Any one of an assortment of foils is inserted into the beam by means of remotely operated actuators in the foil box. After emerging from the gypsy magnet the various hydrogenic charge states drift in a vacuum of 10^{-7} torr for 5.3 m before striking the exit window, where they are completely stripped, and passing through the scintillator telescope. One of two scanning pencil scintillators is used to trace out the distribution of particles.

where $C=\sigma_{-12}/(\sigma_- -\sigma_{12})$, σ_{-12} is the cross section for one electron stripping from H^- into states 1 and 2, and $\sigma_{1,2}$ is the cross section for excitation of the projectile H^0 in 1 or 2 to states $n\geqslant 3$ including continuum states for which H^0 is ionized. For states $n=3$ and above, we add the possibility of contributions from the excitation of 1 or 2. Analogous work has been done for fast H beams passing through gas targets [7]. Thus for $n\geqslant 3$ we have

$$\frac{dy_n(x)}{dx}=\sigma_{-n}\rho y_-(x)-\sigma_n\rho y_n(x)+\sigma_{12n}\rho y_{12}(x), \quad (5)$$

where σ_n is the cross section for excitation from the state n to any other state, including continuum states for which the hydrogen atom loses its electron, and σ_{12n} is the cross section for the excitation from 1 and 2 to n. Thus

$$y_n(x)=A_1e^{-\rho\sigma_- x}+A_2e^{-\rho\sigma_{12}x}+A_3e^{-\rho\sigma_n x}, \quad (6)$$

where

$$A_1=\frac{A(\sigma_{-n}-C\sigma_{12n})}{\sigma_n-\sigma_-}, \quad (7)$$

$$A_2=\frac{AC\sigma_{12n}}{\sigma_n-\sigma_{12}}, \quad (8)$$

and

$$A_3=-(A_1+A_2). \quad (9)$$

For each magnetic field setting, in addition to yields for discrete n's ($n=3$, 4, 5, 6) there are also states that contribute to the spectrum but are not resolved into individual states. For example, $n=3$ shows up clearly at 13 kG, but states with $n\geqslant 4$ are also present as a shoulder on the H^+ peak. These unresolved states are fit along with the resolved n states using Eq. (6).

The proton yield $y_+(x)$ can be fit to the relationship

$$y_+(x)=A-y_-(x)-\sum_n y_n(x). \quad (10)$$

For the higher n states, the peak yield of the state is observed to go as n^{-p} with p being roughly equal to 3 [8]. A theoretical study of double photoionization of two-electron systems at very high photon energies (keV range) finds the same yield dependence for higher n states [9]. The physical basis for the inverse-cube dependence is the radial behavior of the asymptotic Coulomb wave function [10]. In the present study we also examine this phenomenon.

III. EXPERIMENTAL METHOD

We measure the production of excited neutral hydrogen atoms in a foil by studying their trajectories after field ionization in a ramped-field magnet (in which the field increases linearly with distance along the beam line, labeled "gypsy" in Fig. 4). In some cases, the field is strong enough to field strip H^-. The analysis of the H^- stripping seen in these experiments is presented by Keating *et al.* [11]. The ground-state H^0 atoms from the field-stripped H^- arrive at the detection plane in the area between the unstripped H^- and the neutral hydrogen. Likewise, the excited $H^0(n\geqslant 3)$ particles strip and the resultant protons arrive at the detection plane in an area between the unstripped H^0 peak and the H^+ peak. When the atoms in a given H^0 state reach the critical field, given by Eq. (2), they are stripped and the resulting protons follow a curved trajectory due to the downstream magnetic field. The magnet is followed by a 5.3-m drift region and the detector system. Knowing the field map of the magnet (shown in Fig. 5), we can reconstruct the field at which a particular H^0 ionized. This technique and this same magnet were used previously to study the ionization probability of the H^- ground state as a function of field [12].

The experiment took place at the High-Resolution Atomic Beam Facility (HIRAB) at LAMPF where a high-quality H^- beam was available. The beam kinetic energy can be varied from 100 to 800 MeV with typical beam parameters of 2 mm spot size, 100 μrad divergence, and 0.05% $\delta p/p$. With special tuning, these parameters can be improved to <0.5 mm spot size, <10 μrad divergence, and 0.01% $\delta p/p$ [13]. The beam is delivered in 250-ps micropulses spaced by 5 ns bunched in 120, 700-μs macropulses. In the present experiment, measurements were made only at 800 MeV.

The apparatus consists of the foil box, the ramped-field magnet, a 5.3-m flight path, and a detector system. The floor layout is shown in Fig. 4. The particles emerging into air through the aluminum window at the end of the flight path are detected by two large, fixed scintillators and one of two scanning scintillators, one 3.3 mm wide and the other 5.8 mm wide. The scanning scintillator measures the yield of the charge states as determined by the positions in the detector plane of the emerging particles. The large scintillators form a telescope that detects all three charge states of the beam after being stripped so that the particle counts can be normalized. These signals are also put in coincidence with the scanning

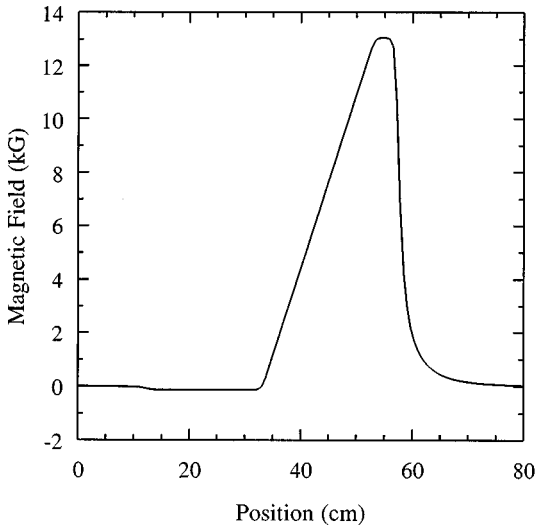

FIG. 5. The transverse magnetic field of the analyzing (gypsy) magnet is plotted vs distance along the beam line. The particles emerging from the foil enter the magnetic field from the left. Depending on the state for which maximum resolution was desired the peak magnetic field was adjusted. In the case shown, the peak field was set to 13 kG for optimal dispersion of the $H^0(3)$ state.

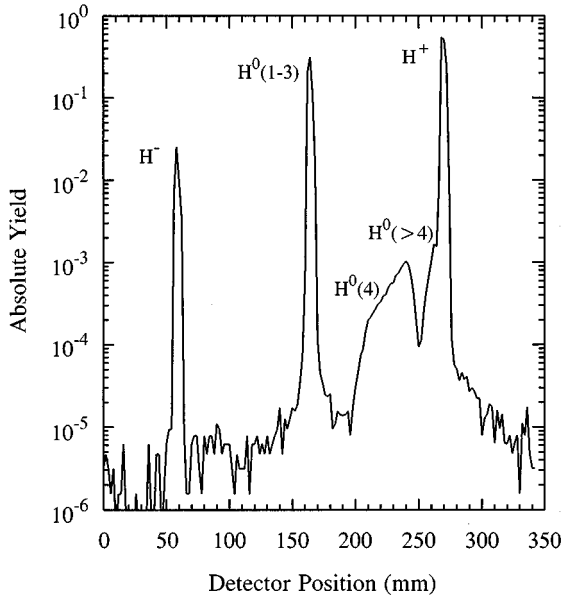

FIG. 6. The count rate on the scanning scintillator, in coincidence with and normalized to the count rate in the telescope, is plotted vs distance transverse to the beam to show the dispersion of particles transmitted through a 100-μg/cm^2 carbon foil. The peak gypsy field is 6 kG to display the $n=4$ states with maximum dispersion. Note the large dynamic range of the count rates vs detector position.

scintillator signal to discriminate against background. Standard beam diagnostics along the beam line and phase-space tailoring apparatus of the incident beam are not shown.

The carbon foils are commercial foils from Arizona Carbon Foil Company, produced with a tolerance on the thickness of $\pm 10\%$. We used an α-ranging technique to more precisely estimate the foil thicknesses and uncertainties [14]. The carbon foils are floated onto metal frames with 2-cm-diam holes for the thicker foils (>40 μg/cm^2), or 1.3 cm for the thinner foils. These foils are all free-hanging so there is nothing else in the interaction area to affect the H^- beam. The aluminum oxide foils are produced at Rutherford Appleton Laboratory to be used as stripper foils, and are already mounted to frames on an aperture 2 cm in diameter.

The ramped-field magnet is a half quadrupole turned sideways to the beam. The beam enters through a hole in the return yoke and then encounters the vertical magnetic field (perpendicular to the beam) whose strength increases linearly along the beam axis. The maximum field available is 1.9 T and the length of the ramped region is 0.2 m. A field of 1.9 T is not enough to strip $n=2$, so the maximum setting used is 1.3 to strip $n=3$.

The yield at each position of the scanning scintillator is the quotient of the signal from the scanning scintillator to the total signal received by the scintillator telescope. A spectrum consists of the yield vs position of the scanning scintillator. Examples of such spectra are shown in Figs. 6 and 7. Notice that these spectra have a large dynamic range, up to six orders of magnitude. The leftmost peak is from the H^- ions. Figure 6, with the gypsy magnet set to 6 kG, shows little H^- field stripping; Fig. 7, with the gypsy magnet set to 13 kG, shows that for this large magnetic field most of the H^- surviving the foil are field stripped. The large central peak is from the neutral hydrogens that are in states too low to be field stripped. The high peak on the right side of the spectrum is from the protons. The low, wide peak between the neutrals and the proton peak is from the H^- ions that were stripped to excited-state H^0 atoms that were subsequently field stripped by the gypsy magnet. Different Stark substrates within the same n manifold will strip at different magnetic field strengths, causing the observed spread in the peak. The shoulder on the proton peak is due to the field stripping of higher excited states that cannot be individually resolved. The absolute yield of a particular species for one foil thickness is then defined operationally as the integrated area of the part of the yield spectrum attributed to that species divided by the integrated area of the whole spectrum. We also took into account spontaneous decay from the excited states in the drift region between the foil and the magnetic field. The method used for estimating the decay is discussed in Keating *et al.* [15]. The normalization to the area of the whole spectrum is necessary to avoid double counting due to overlap of the scanning scintillator signal from point to point. Physically the absolute yield of a particular species then represents the yield per H^- ion.

IV. RESULTS AND CONCLUSIONS

A. Yields

We determined yield vs foil thickness for carbon foils for the H^-, H^0 ($n=1$, 2), and H^+ peaks. In addition we obtained yield as a function of foil thickness for $n=3$, 4, 5, 6, and for $n>6$ (which would be mostly made up of $n=7$). Yields for the carbon foils are plotted vs thickness in Figs. 8–10. A smaller data set was obtained for Al_2O_3 foils. The best-fit curves through the data were obtained via a least-squares

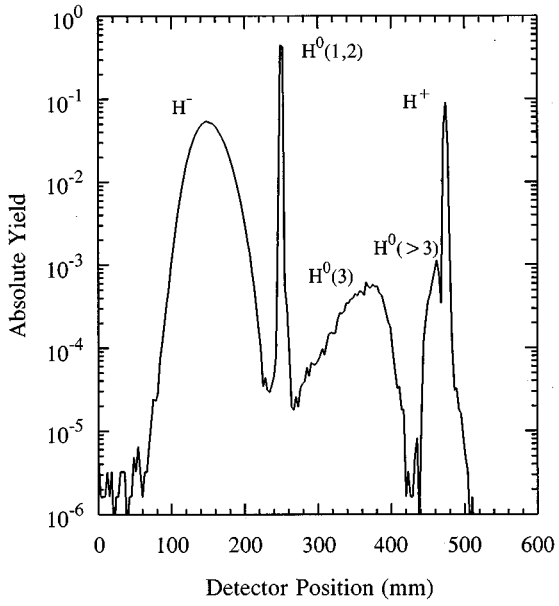

FIG. 7. Absolute yields at a maximum gypsy field of 13 kG and a 20-μg/cm^2 carbon foil showing the three main peaks and the H^0 ($n=3$) peak separated with optimal dispersion. Also seen is the H^0 ($n>3$) peak just barely separated from the proton peak. The 13-kG field is strong enough to field strip the H^- ions that passed through the foil intact, producing the wide spread of the H^- peak. This is examined more closely by Keating *et al.* [11].

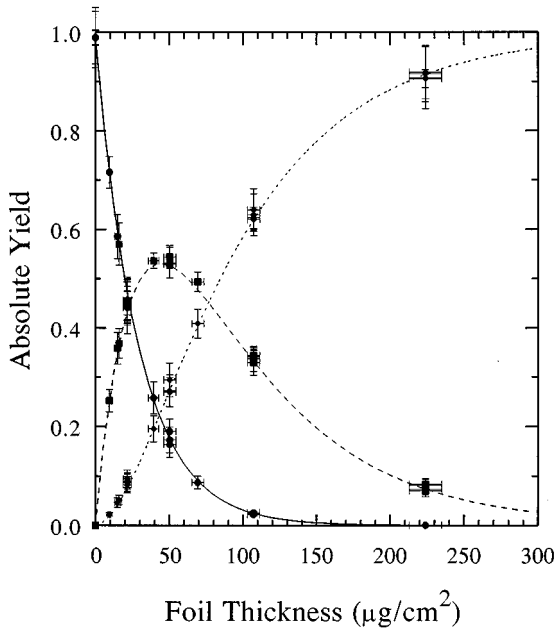

FIG. 8. Experimental data and best fits of H^- (solid line through circles), H^0 (dashed line through squares), and H^+ (dotted line through diamonds) yields vs carbon foil thickness. The multiple points represent the different magnetic field settings used in the experiment so that all the charge state data are shown.

fitting routine using the Levenberg-Marquardt method as discussed by Press *et al.* [16]. The fitting parameters are the cross sections for the various processes.

B. Cross sections

1. Charge state cross sections

We first fit the data to just the overall charge states to obtain σ_{-0}, σ_{-+}, and σ_{0+}, using Eqs. (3), (4), and (10). The best-fit values for the cross sections are reported in Table I. The χ^2 for this fit was 18.3 with 58 degrees of freedom, indicating a confident fit. It is significant that we were able to find a value for σ_{-+} for carbon that was larger than the uncertainty; our estimate of the branching ratio of double to single ionization is (1.8±0.9)%. The uncertainty in this ratio is due primarily to the uncertainty in σ_{-+}. The estimated uncertainties come from the diagonal elements of the covariance matrix associated with the best fit. The major sources of uncertainty include statistical fluctuations, the detector response, and uncertainties in foil thickness. The foil thicknesses were measured by α ranging [14]. The aluminum oxide values are less certain because we obtained fewer data points. The stripping lengths λ corresponding to the cross sections for carbon reported in Table I ($\lambda_{-0}=29.6\pm0.4$ μg/cm^2 and $\lambda_{0+}=75.8\pm1.4$ μg/cm^2) can also be compared to the values obtained by van Dyck [17] for Formvar ($C_3H_7O_2$) foils of $\lambda_-=30\pm3$ μg/cm^2 and $\lambda_0=60\pm6$ μg/cm^2.

2. Some individual state cross sections

We examined the entire spectrum, including the excited-state peaks, at a particular peak magnetic field. The yields vs foil thickness were fit using Eqs. (3) for H^-, (4) for H^0 ($n=1$, 2), (6) for the excited-state peaks and (10) for H^-, and the cross sections derived from the best-fit parameters. Table II reports the cross sections obtained for the different magnetic field settings. Note that some of the quoted cross sections are

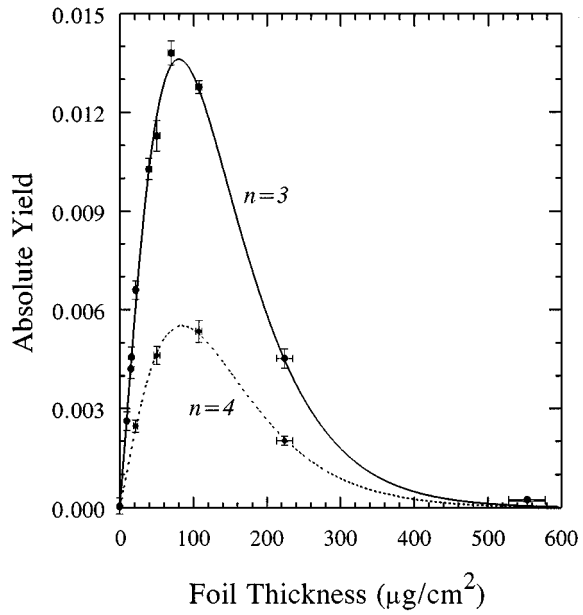

FIG. 9. H^0 ($n=3$) yield, represented by the circles, and H^0 ($n=4$) yield, represented by the diamonds, vs carbon foil thickness. The $n=3$ data were taken at a maximum gypsy magnetic field of 13 kG and the $n=4$ at 6 kG. The lines are from the best fit of Eq. (6) to the data.

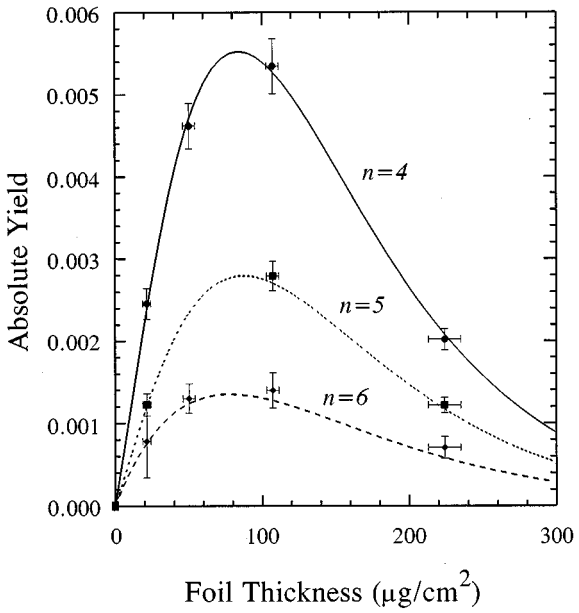

FIG. 10. H^0 ($n=4$) yield, represented by the circles, H^0 ($n=5$) yield, represented by the squares, and H^0 ($n=6$) yield, represented by the diamonds, vs carbon foil thickness. The lines are the best fit of Eq. (6) to these data. The $H^0(4)$ yield is the same as that shown in Fig. 9, reproduced here to give the reader a better sense of the relative sizes of the different excited-state yields.

actually weighted averages. For example, σ_{123n} is not simply the sum of σ_{12n} and σ_{3n}. For the 13-kG magnetic field, the χ^2 is 14 with 40 degrees of freedom, giving a reduced χ^2 of 0.35 and a high confidence level. For the 6-kG magnetic field the χ^2 is 9.2 with 10 degrees of freedom, giving a reduced χ^2 of 0.92 and a confidence level of 51%. Both the 2.9- and 1.6-kG magnetic field fits, with relatively large uncertainties in the data, have χ^2 values less than 1, giving very confident fits. For the 1.6-kG case in particular, it is possible that there is a significant amount of mixing of the $n=6$ and 7 yields.

A few measurements were conducted using aluminum oxide (Al_2O_3) foils. We did not have as many thicknesses over which to produce the yield curves, but some preliminary results were obtained. The method of analysis was the same as that for the carbon foils. We obtained yield curves and cross sections for H^-, H^0 ($n=1$, 2), H^0 ($n=3$), H^0 ($n>3$), and H^+ for the aluminum oxide. The yield curves are shown in Figs. 11 and 12. The cross sections are in Table III. The χ^2 is 2.8 with 5 degrees of freedom and a confidence level of 73%. A comparison of the $n=3$ yields for carbon and aluminum oxide are shown in Fig. 13. The yield of $n=3$ for Al_2O_3 is less than that of carbon, implying that aluminum oxide may be a good material for beam stripping.

TABLE I. Charge state cross sections.

Foil	σ_{-0} (10^{-19} cm^2)	σ_{-+} (10^{-19} cm^2)	σ_{0+} (10^{-19} cm^2)
Carbon	6.76±0.09	0.12±0.06	2.64±0.05
Aluminum oxide	12±1	<1.5	5.3±0.3

TABLE II. Cross sections for carbon. (a) 13 kG. (b) 6 kG. (c) 2.9 kG. (d) 1.6 kG.

Designation	Initial state	Final state	Cross section (10^{-19} cm^2)
		(a)	
σ_-	−	0,+	6.87±0.16
σ_{-12}	−	1,2	6.68±0.15
σ_{12}	1,2	anything else	2.75±0.10
σ_{-3}	−	3	0.053±0.005
σ_3	3	anything else	4.5±0.4
σ_{123}	1,2	3	0.13±0.01
$\sigma_{->3}$	−	>3	0.02±0.002
$\sigma_{>3}$	>3	anything else	2.6±0.3
$\sigma_{12>3}$	1,2	>3	0.033±0.003
σ_{-+}	−	+	0.11±0.08
σ_{12+}	1,2	+	2.6±0.1
		(b)	
σ_-	−	0,+	7.22±0.35
σ_{-123}	−	1,2,3	6.98±0.34
σ_{123}	1,2,3	anything else	2.80±0.17
σ_{-4}	−	4	0.021±0.005
σ_4	4	anything else	3.69±0.56
σ_{1234}	1,2,3	4	0.046±0.009
$\sigma_{->4}$	−	>4	0.0086±0.002
$\sigma_{>4}$	>4	anything else	2.5±0.4
$\sigma_{123>4}$	1,2,3	>4	0.016±0.003
σ_{-+}	−	+	<0.42
σ_{123+}	1,2,3	+	2.74±0.17
		(c)	
σ_-	−	0,+	7.05±0.35
σ_{-1234}	−	1−4	6.94±0.35
σ_{1234}	1−4	anything else	2.74±0.17
σ_{-5}	−	5	0.011±0.006
σ_5	5	anything else	3.2±1.2
σ_{12345}	1−4	5	0.021±0.011
σ_{-+}	−	+	<0.36
σ_{1234+}	1−4	+	2.72±0.16
		(d)	
σ_-	−	0,+	6.91±0.27
σ_{-12345}	−	1−5	6.68±0.26
σ_{12345}	1−5	anything else	2.64±0.13
σ_{-6}	−	6	0.0093±0.0055
σ_6	6	anything else	2.3±1.6
σ_{123456}	1−5	6	<0.014
$\sigma_{->6}$	−	>6	<0.01
$\sigma_{>6}$	>6	anything else	<4.8
$\sigma_{12345>6}$	1−5	>6	<0.026
σ_{-+}	−	+	<0.19
σ_{12345+}	1−5	+	2.62±0.13

C. Cross sections vs *n*

For the carbon foils, the cross sections σ_{-n} and σ_{12n} were plotted vs the principal quantum number n (Figs. 14 and 15)

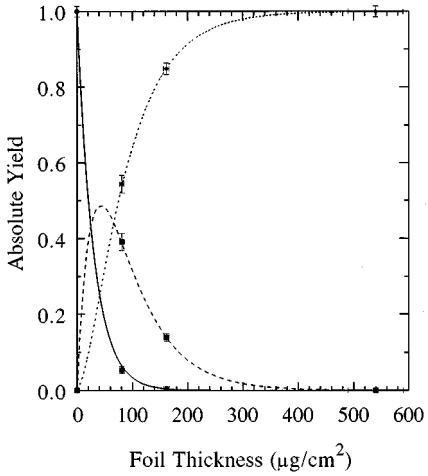

FIG. 11. H^- (solid line), H^0 (dashed line), and H^- (dotted line) yields vs Al_2O_3 foil thickness in analogy to Fig. 8. Notice that the peak of the H^0 yield is not as high as that for the carbon foils.

and fit to $\sigma(n)=An^{-p}$. For σ_{-n}, the best-fit value for p is 2.8 ± 0.4; for $\sigma_{1,2n}p$ is 3.5 ± 0.4, consistent with an n^{-3} dependence.

D. Comparisons to earlier work

We found that the peak yield for $n\geqslant3$ states occurs at a foil thickness that is substantially thicker than the peak for the $n=1$, 2 yield, in agreement with the earlier work of Mohagheghi *et al.* [1], as shown in Fig. 16. We have also plotted estimates of the positions of maxima taken from the accompanying theoretical paper by Gervais, Reinhold, and Burgdörfer [2]. The peak of the yield for $n=1$, 2 occurs at around 40 μg/cm^2, whereas the peaks for greater values of n occur at thicknesses ranging from 70 to 90 μg/cm^2. The improved "simple model" [Eq. (6)] for the higher n values that takes into account the excitation of the $n=1$, 2 states helps to explain this. The atoms in the $n=1$, 2 states are produced by H^- stripping directly to those states, but for the higher excited states, there are a significant number of atoms that reach that state by first being stripped from H^- to $H^0(1,2)$ and then being excited to the higher state. Although Mohagheghi *et al.* [1] were able to measure the relative yield of $n=2$ vs foil thickness and to demonstrate that its dependence is similar to $n=1$, i.e., a maximum yield at about 40 μg/cm^2, the absolute yield was not determined. Moreover, the ratio of $n=2$ to $n=1$ production has not been measured. Calculations

TABLE III. 13-kG cross sections for aluminum oxide.

Designation	Initial state	Final state	Cross section (10^{-19} cm^2)
σ_-	−	0,+	12.4±1.4
σ_{-12}	−	1,2	12±1
σ_{12}	1,2	anything else	5.7±0.4
σ_{-3}	−	3	0.15±0.02
σ_3	3	anything else	4.2±0.2
σ_{123}	1,2	3	0.055±0.012
$\sigma_{\to3}$	−	>3	0.060±0.008
$\sigma_{>3}$	>3	anything else	1.9±0.1
$\sigma_{12>3}$	1,2	>3	0.0066±0.0046
σ_{-+}	−	+	<1.1
σ_{12+}	1,2	+	5.7±0.4

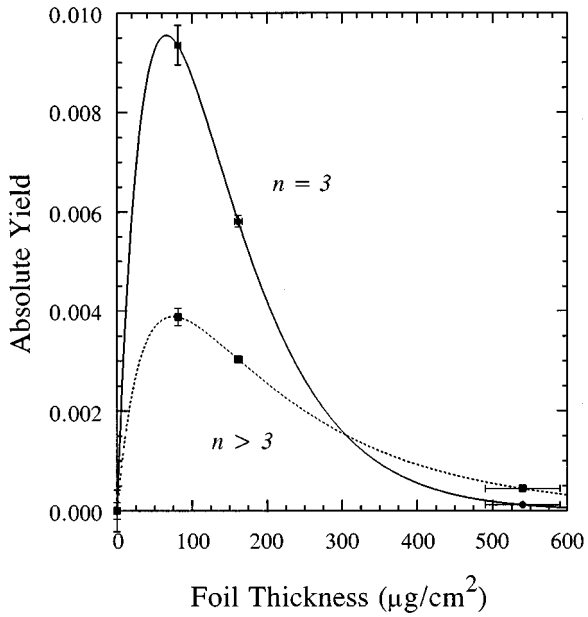

FIG. 12. H^0 ($n=3$) yield and H^0 ($n>3$) yield vs Al_2O_3 foil thickness.

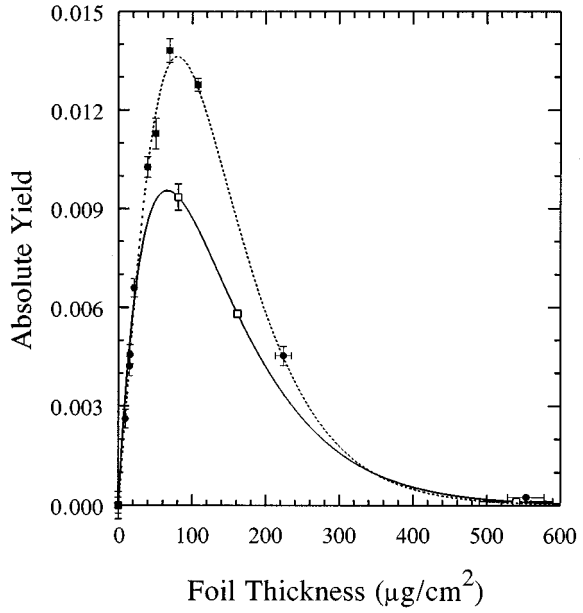

FIG. 13. Comparison of H^0 ($n=3$) yield for carbon (dotted lines and diamonds) and Al_2O_3 (solid lines and squares). The height of the Al_2O_3 peak is about 70% of the height of the carbon peak. The foil thickness at which the Al_2O_3 peaks is also less than that of the carbon, and less well determined.

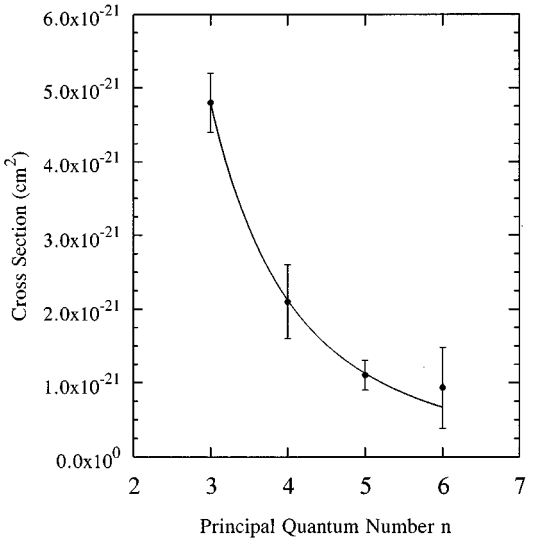

FIG. 14. Cross section for stripping from H^- to $H^0(n)$ vs the principal quantum number n. The line is the best fit to $\sigma\alpha n^{-p}$, with $p=2.8\pm0.4$.

by Dalgarno and Sadeghpour [9] indicate that this ratio for photoionization in the high-energy limit is anomalously large (0.66) for H^- vs other two-electron systems (He and Li^+), presumably due to the broad doubly excited shape resonance in H^-. Gervais, Reinhold, and Burgdörfer [2] find the two yield curves to be indeed very similar in the region of the maximum, corresponding to a ratio of about 0.24. Other theoretical studies of the relative production rates of the first excited state to the ground state of hydrogen in collisional electron detachment processes from H^- confirm that the ratio is anomalously large [7,18–20]. As one might expect, the yield curves [1,2] for large foil thicknesses for these two states indicate the destruction of $n=2$ has a larger cross section than for $n=1$. Therefore our experimentally derived

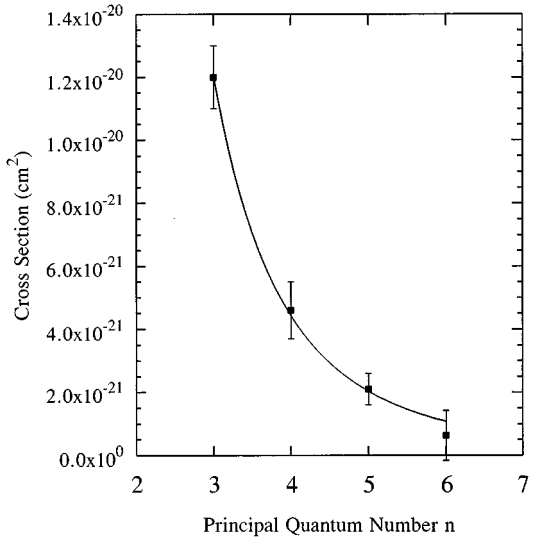

FIG. 15. Cross section for excitation from $H^0(1,2)$ to $H^0(n)$ vs the principal quantum number n. The line is the best fit to $\sigma\alpha n^{-p}$, with $p=3.5\pm0.4$.

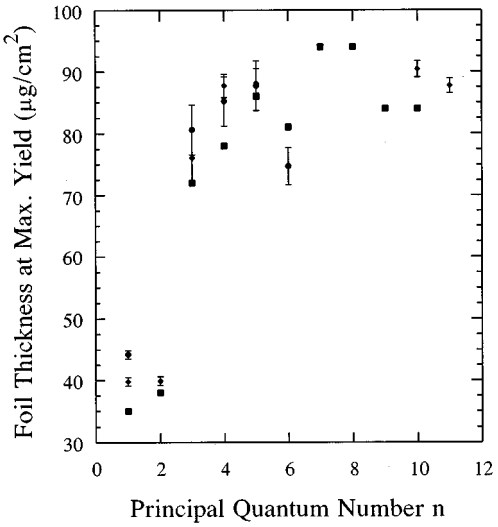

FIG. 16. Foil thickness for the peak yield of $H^0(n)$ in a carbon foil vs principal quantum number n. The diamonds are from the data of Mohagheghi *et al.* [1], the circles are from the present study, and the squares are theoretical estimates read from the Monte Carlo graphs of Gervais, Reinhold, and Burgdörfer [2]. The large difference between $n=1$ and 2 and the higher values of n is due to the contribution of the two-step process in which $H^0(1,2)$ from stripped H^- gets excited to $H^0(n)$.

cross sections, σ_{12}, must be regarded as merely a parameter, approximating an average cross section for two processes whose weighting depends on foil thickness.

Figures 17 and 18 show combined yield curves that include the data of Mohagheghi *et al.* for $n=1,2$ and for $n=3$ with the data from the present study. The data of Mohagheghi *et al.* are normalized to our data, treating the normalization as another fitting parameter.

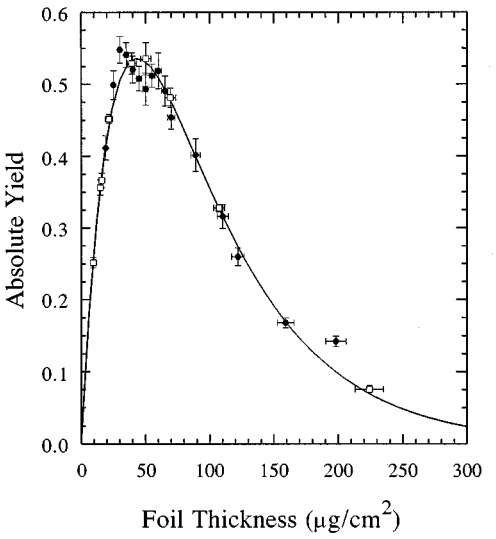

FIG. 17. Yield of $H^0(1,2)$ vs foil thickness for carbon; the circles are from Mohagheghi *et al.* [1], normalized to our results by a parameter in the fitting routine, and the squares are from the present study. The line is a best fit to all of the data and the results are consistent with the best fit obtained using just our data.

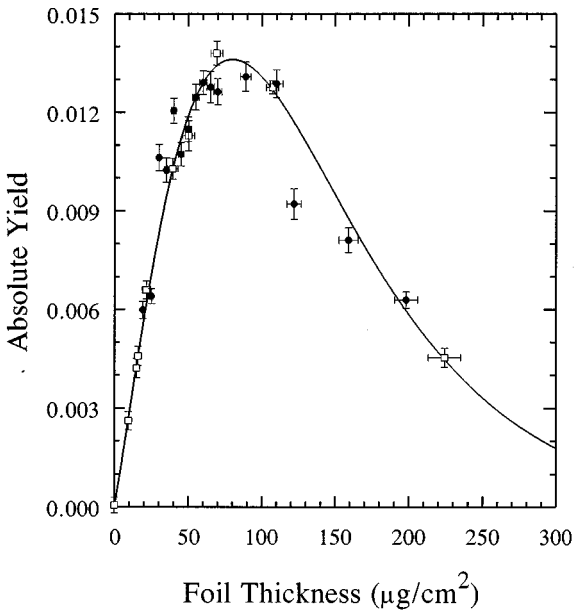

FIG. 18. Yield of $H^0(3)$ vs foil thickness for carbon; as in Fig. 17, the circles are from Mohagheghi *et al.* [1], normalized to our results by a parameter in the fitting routine, and the squares are from the present study. The line is a best fit to all of the data and the results are also consistent with the best fit obtained using just our data.

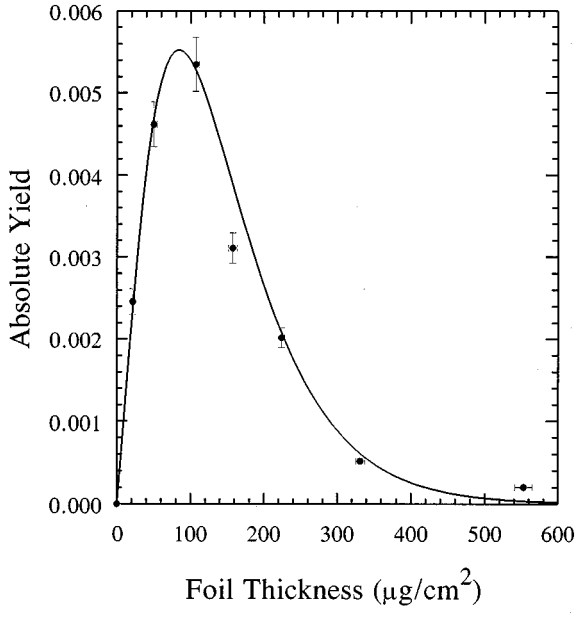

FIG. 19. $H^0(4)$ yield vs carbon foil thickness. Here the line is a best fit to the single-foil data points. The double-foil data points are shown at 157 and 320 μg/cm^2 and demonstrate that they are systematically low in comparison to the best fit obtained with just the single-foil data.

E. Double-foil discrepancies

It has been suggested that the yields of two closely spaced foils, one after the other, will not be the same as that of a single foil of the same total thickness [21]. Double-foil experiments are often suggested and even tried in the field of beam-foil spectroscopy. For example, see Betz *et al.* [22]. During this experiment we made a preliminary test of this hypothesis. For the 13- and 6-kG set of runs, we made an equivalent thicker foil by placing two thinner foils into the interaction region, one in front of the other, separated by roughly 1 cm. In all cases, the two foils were not the same thickness; usually it was a 200- and a 100-μg/cm^2 foil (in both the 13- and 6-kG runs) or a 100- and a 50-μg/cm^2 foil (in the 6-kG set only). These double foils gave $H^0(n)$ yields that were lower than expected from the single-foil data alone. Figure 19 shows the $n=4$ data and the best-fit curve for which data from the double foils were not used. The two double-foil data points at 157 and 320 μg/cm^2 are low in relation to the single-foil data points and the best-fit yield curve derived from the single-foil data. When the double foils were included in the data analysis, the χ^2 was 22.8 for 20 degrees of freedom, giving a reduced χ^2 of 1.14 and a confidence level of 30%. With the composite foils removed from the data, the χ^2 was 9.2 (10 degrees of freedom), producing a reduced χ^2 of 0.92 and a confidence level of 51%. While this is not decisive evidence that the yields of two closely spaced foils, one after the other, will not be the same as that of a single foil of the same total thickness, it does suggest that a more detailed study of this phenomenon might give new insight into the physics of foil stripping.

F. Conclusions

We measured absolute yield vs foil thickness for H^-, H^0, and H^+ in both carbon and Al_2O_3 foils. In the case of carbon, we determined yield distributions for H^0 ($n=3$, 4, 5, 6). For the Al_2O_3 we found yields for $H^0(3)$ and $H^0(>3)$. From the fits to these yields vs thickness, we obtained values for a number of cross sections associated with this stripping process and found the double to single ionization ratio. The description of the passage of H^- through foils parametrized in terms of cross sections is adequate for our data, and the addition of two-step processes into the model [Eq. (6)] vastly improves the agreement between the model and experiment over previous attempts. We improved the accuracy of the carbon foil values over previous reports and presented aluminum oxide values at a beam energy of 800 MeV. The interesting question of the nature of the mechanism that ties together the $n=1$ and 2 production rates in a foil remains open.

ACKNOWLEDGMENTS

The authors would like to acknowledge technical support from Lawrence Quintana, Larry Rybarcyk, John Gomez, Fred Roybal, Mike Borden, Kevin Jones, and John O'Donnell at Los Alamos, and from Jim Hontas at the University of New Mexico. Joseph Macek, Tom Bergeman, Péter Kálmán, János Bergou, and Joachim Burgdörfer were helpful with theoretical discussions. This work was supported by the U.S. Department of Energy, in part by the Division of Chemical Sciences, Office of Basic Energy Sciences, Office of Energy Research.

[1] A. H. Mohagheghi *et al.*, Phys. Rev. A **43**, 1345 (1991).
[2] B. Gervais, C. Reinhold, and J. Burgdörfer, preceding paper, Phys. Rev. A **53**, 3190 (1996).
[3] Richard Hutson, Los Alamos National Laboratory Report No. PSR-92-015, 1992 (unpublished).
[4] R. J. Macek in *Proceedings of the XIIth Meeting of the International Collaboration on Advanced Neutron Sources, Abingdon, Oxfordshire, UK, 1993*, edited by U. Steigenberger *et al.* (Science and Engineering Research Council, Rutheford Appleton Laboratory, Chilton, 1993), Vol. II, pp. A25–A32.
[5] J. D. Jackson, *Classical Electrodynamics*, 2nd ed. (Wiley, New York, 1975).
[6] T. F. Gallagher, Rep. Prog. Phys. **51**, 154 (1988).
[7] G. H. Gillespie, Nucl. Instrum. Methods Phys. Res. Sect. B **2**, 231 (1984).
[8] A. H. Mohagheghi, Ph.D. thesis, University of New Mexico, 1990.
[9] A. Dalgarno and H. R. Sadeghpour, Phys. Rev. A **46**, R3591 (1992).
[10] H. Friedrich, *Theoretical Atomic Physics* (Springer-Verlag, Berlin, 1990).
[11] P. B. Keating *et al.*, Phys. Rev. A **52**, 1 (1995).
[12] A. J. Jason, D. W. Hudgings, and O. B. van Dyck, Los Alamos National Laboratory Report No. LA-UR-81-831, 1981 (unpublished).
[13] P. G. Harris *et al.*, Nucl. Instrum. Methods Phys. Res. Sect. A **292**, 254 (1990).
[14] M. S. Gulley and W. A. Miller, Los Alamos National Laboratory Report No. LA-UR-95-2110, 1995 (unpublished).
[15] P. B. Keating *et al.* (unpublished).
[16] W. H. Press, B. P. Flannery, S. A. Teukolsky, and W. T. Veuerling, *Numerical Recipes* (Cambridge University Press, Cambridge, England, 1989), Chap. 14.
[17] O. van Dyck, IEEE Trans. Nucl. Sci. **NS-26**, 3992 (1979).
[18] G. H. Gillespie, Nucl. Instrum. Methods Phys. Res. Sect. B **10/11**, 22 (1985).
[19] L. A. Wright, M. R. Franz, and T. C. Genoni, Phys. Rev. A **32**, 1215 (1985).
[20] G. H. Gillespie, R. S. Janda, and D. L. Moores, in *Abstracts of Contributed Papers, Proceedings of the XIIIth International Conference on the Physics of Electronic and Atomic Collisions, Berlin, 1983*, edited by J. Eichler *et al.* (International Conference on the Physics of Electronic and Atomic Collisions, Berlin, 1984), p. 402.
[21] Vadim Dudnikov (private communication).
[22] H. D. Betz *et al.*, Nucl. Instrum. Methods Phys. Res. Sect. B **33**, 185 (1988).